Article type: Full Paper

Organic-based Field Effect Transistors for Protein Detection fabricated by Inkjet-Printing

*Carme Martínez-Domingo, Silvia Conti, Alfredo de la Escosura-Muñiz, Lluís Terés, Arben Merkoçi and Eloi Ramon **

Dr. Carme Martínez-Domingo, Dr. Silvia Conti, Dr. Lluís Terés, Dr. Eloi Ramon
Institut de Microelectrònica de Barcelona IMB-CNM (CSIC). Campus de la UAB, 08193 Bellaterra, Catalonia, Spain.
E-mail: eloi.ramon@imb-cnm.csic.es

Dr. Silvia Conti
Dipartimento di Ingegneria dell'Informazione, University of Pisa
56122, Pisa, Italy

Dr. Alfredo de la Escosura-Muñiz, Prof. Arben Merkoçi
Catalan Institute of Nanoscience and Nanotechnology (ICN2), CSIC and Barcelona Institute of Science and Technology, Campus UAB, 08193 Barcelona, Spain.

Prof. Arben Merkoçi
ICREA—Institució Catalana de Recerca i Estudis Avançats, Pg. Lluís Companys 23, 08010 Barcelona, Spain.

Keywords: organic electronics, inkjet-printing, thin-film transistor, surface functionalization

Abstract

Biosensors based on Organic Field-Effect Transistors (OFETs) have attracted increasing attention due to the possibility of rapid, label-free, and inexpensive detection. Among all the different possibilities, inkjet-printed top-gate organic Field Effect Transistors-Based Biosensors (BioFETs) using a polymeric gate insulator have been seldom reported. In this work, a systematic investigation in terms of topographical and electrical characterization was carried out in order to find the optimal fabrication process for obtaining a reliable polymer insulator. Previous studies have demonstrated that the best electrical performance arises from the use of the perfluoropolymer Cytop^{TM}.[1],[2],[3] Consequently, a simple immobilization protocol was used to ensure the proper attachment of a model biomolecule onto the Cytop's

hydrophobic surface whilst keeping its remarkable insulating properties with gate current in the range of dozens of pico-ampers. The top-gate inkjet-printed BioFETs presented in this study operate at threshold voltages in the range of 1-2 V and show durability even when exposed to oxygen plasma, wet amine functionalization treatments, and aqueous media. As a preliminary application, the inkjet-printed top-gate BioFETs is used for monitoring an immunoreaction by measuring changes in the drain current, paving the way for further use of this device in the immunosensing field.

1. Introduction

Currently, the emerging field of organic electronics is driven by the possibility of achieving mass-scale production by using, for example, printing techniques. As opposed to the more conventional processes, over last years, inkjet-printing has received a keen interest as a versatile approach for the deposition of small amounts of functional materials, as small molecule dispersions, polymer solutions, or nanoparticle suspensions, that possess specific electrical, optical, and chemical properties onto well-defined areas of various surfaces and substrates.[4] Moreover, inkjet-printing technology is well suited for research, being a mask-less technology oriented to rapid prototyping for production.[5]

The considerable effort made to optimize Organic Semiconductors (OSCs) has led to the development of Organic Field Effect Transistors (OFETs) that have the potential to be used as transducers for biological and chemical sensors. The most reported BioFETs are based on Organic Electrochemical Transistors (OECTs), and Electrolyte Gated OFETs (EGOFETs).[6],[7] In these structures, the detection relies on the functionalization of the OSC layer, which interfaces with an electrolytic solution. However, one of the main disadvantages of these approaches is the possible degradation of the OSC caused by its direct exposure to aqueous media. Extended Gate Field-Effect Transistors (EGFETs) where an

elongated gate is separated from the transistor were proposed to solve this problem.[8] However, main drawbacks of EGFET arise from the increase of the manufacturing processes and enlarged device dimensions impacting its integration.

In the herein proposed top-gate bottom-contact BioFET structure, the OSC is not directly exposed to the sensing environment as it is protected by the dielectric, which is in direct contact with the medium to be analyzed. The bio-recognition element is anchored onto the dielectric surface, which acts as the sensing area. This configuration ensures field-effect operation without charge transfer, between the electrolyte and the OSC, blocking the passage of the current which could promote electrochemical reactions such as hydrolysis. This approach has shown good performances thanks to good operational and environmental stability.[9] The main requirement to operate and to properly transduce this binding event is an effective gate coupling between the insulator and the OSC via a field-effect resulting from a good electrical insulator. Thus, it is imperative to study and develop carefully engineered gate dielectrics that can reliably operate at relatively high electric fields.

Polymers can be deposited fairly easily as thin films using solution-based deposition techniques while their low thermal properties make them highly compatible with plastic substrates. Numerous works have studied the electrical performance and relative ageing of functional polymers when they are used as gate insulators or encapsulation layers.[10],[11] However, the reliability of bio-functionalized insulating polymers employed in top-gate BioFET structures in relation to the leakage of current across them under relatively high electric fields, is still under-represented in the literature. Moreover, the stability of biomolecule immobilization onto sensing areas needs to be assured in top-gate BioFET devices. To obtain a stable attachment, the formation of a covalent bond between the biomolecule and the surface is required. These functionalization methods generally require salt-based buffers, organic solvents, and frequently, oxygen plasma treatments that can

promote the diffusion of mobile ions inside the polymers causing physical and/or chemical interactions producing electrical breakdowns, making it difficult to obtain reliable BioFETs. [12],[13],[14]

In this context, we present a systematic study on a novel, organic inkjet-printed top-gate BioFET that uses a perfluoropolymeric material as both the gate insulator and the transducing layer. Perfluoropolymers are the most used insulating polymers as barrier layers in order to protect the OSCs against environmental conditions. These materials present interesting characteristics, such as high electrical breakdown and low water absorption, thanks to weak dispersive interactions of fluorocarbons, dipolar cancellation and lack of polarizability that are conferred by C-F bonds in perfluorocarbon compounds, making them a good choice for top-gate OFET and BioFET applications.[1],[15],[30] At the same time, because of their hydrophobic nature, the grafting of biomolecules on their surfaces is challenging. Seldom have top-gate BioFETs been reported using perfluoropolymers as the gate insulator. Most of them employ conventional, expensive, and time-consuming techniques, such as Chemical Vapor Deposition (CVD), Plasma Enhanced-CVD (PE-CVD) and high temperatures,[10],[16] to functionalize these materials. Thus, a deep insight into gate dielectric perfluoropolymers-based materials needed to be carried out to ensure a proper functionalization of their surfaces using cost-effective methods without affecting their insulating properties. Amorphous perfluoropolymer dielectric (Cytop^{TM}) was selected for its favourable insulating properties and used to subsequently develop a functionalized top-gate BioFET. Moreover, the immobilization of the receptors onto the insulator by covalent bonding can be achieved using a very simple method involving a model protein. The main advantage of the proposed methodology is that it does not require any specialized equipment and thus, can be conducted in most laboratories. Finally, to demonstrate as a proof-of-concept

that the developed procedure can be used in immunosensing analysis, the detection of the model antigen HIgG was carried out to propel the device into this research field.

2. Results and Discussion

2.1. Assessment of organic dielectrics for top-gate BioFETs

The well-known commercial perfluoropolymer Cytop was used in this study. For comparison purpose, other commonly used organic insulators such as cross-linked poly(4-vinylphenol) (cPVP),[17],[18] epoxy (SU-8),[19],[20] and poly(methyl methacrylate) (PMMA),[21] were evaluated due to their good insulating characteristics and low-temperature processing.

It is known that ions from aqueous solutions and salt-based buffers, typical analysis media used with biological samples, can penetrate into polymer films producing breakdowns.[22],[23] The main goal of this work was to engineer a reliable gate polymeric dielectric which can operate in aqueous media. Thus, the performances of the dielectrics under these conditions were investigated at the beginning of the study. Metal/Insulator/Electrolyte (MIE) capacitors were fabricated for each insulator using an inkjet-printed metallic bottom electrode. cPVP, SU-8, PMMA, and Cytop were deposited by the spin-coating technique. **Figure S1**A (see *supporting information*) shows the MIE structure and the molecular structures of each polymer. An electrolytic solution based on Phosphate Buffer Saline (PBS), the most common biological buffer, was placed on top of the insulators. The polarization of the electrolyte was done by immersing a platinum (Pt) wire into the electrolyte as can be seen in Figure S1B. The resistance values measured for each dielectric are shown in Figure S1C. Impedance Spectroscopy analysis was carried out on these structures to study the resistance of the MIE capacitors. Furthermore, the process yield calculated over 25 capacitors for each dielectric was considered as a parameter for good fabrication methodology. The thicknesses of all the dielectrics were in the range of 800 nm – 1 µm. The cPVP structure presented a low resistance and poor fabrication yield; more than

80% had short-circuited. For SU-8, the obtained resistance was the one of a fairly good insulator (10^9 Ω) but it failed as an strong dielectric with a yield of 80 %. Cytop and PMMA dielectrics presented the highest resistance of 10^{10} Ω. The PMMA layer had process yield 70 %, while the Cytop presented values of almost 100 %, thus assuring reliable devices. In view of the electrical performances of the presented insulators, Cytop was chosen as the best candidate for developing the top-gate BioFETs used in this study.

2.2. Electrical and morphological study of perfluoropolymer dielectric for top-gate BioFETs

As already underlined in the introduction, a good transduction of the binding event through an effective capacitive coupling is fundamental for obtaining a good sensor response. The electrical coupling depends, amongst others, on the film thickness (*d*) which is a convenient parameter because it can be easily controlled during the fabrication process. Thinner dielectric films will result in higher capacitance values and lower operating voltages. In order to find a good compromise between the Cytop thickness and the absence of electrical breakdown, an in-depth study on different thicknesses, surface topography, capacitance and leakage current was carried out on the MIE structures. The dielectric was spin-coated onto the inkjet-printed metallic electrodes at 500 rpm, 1000 rpm, 1500 rpm, and 2000 rpm. Spin coating technique was chosen in order to employ the same deposition techniques for all the dielectrics since the high viscosity of the Cytop is not compatible with inkjet-printing deposition. Furthermore, dilutions of Cytop for adapting it to printing technology were carried out (results not presented here) but electrical measurement on MIE structures presented undoubtedly short-circuits. The *C-V* curves provide information about the leakage current across the insulator. Additionally, in order to study the degradation of the performances under electrical stress cycles, *C-Vs* measurements were recorded repeatedly (named as ‘append’, see **Figure 1**.i).

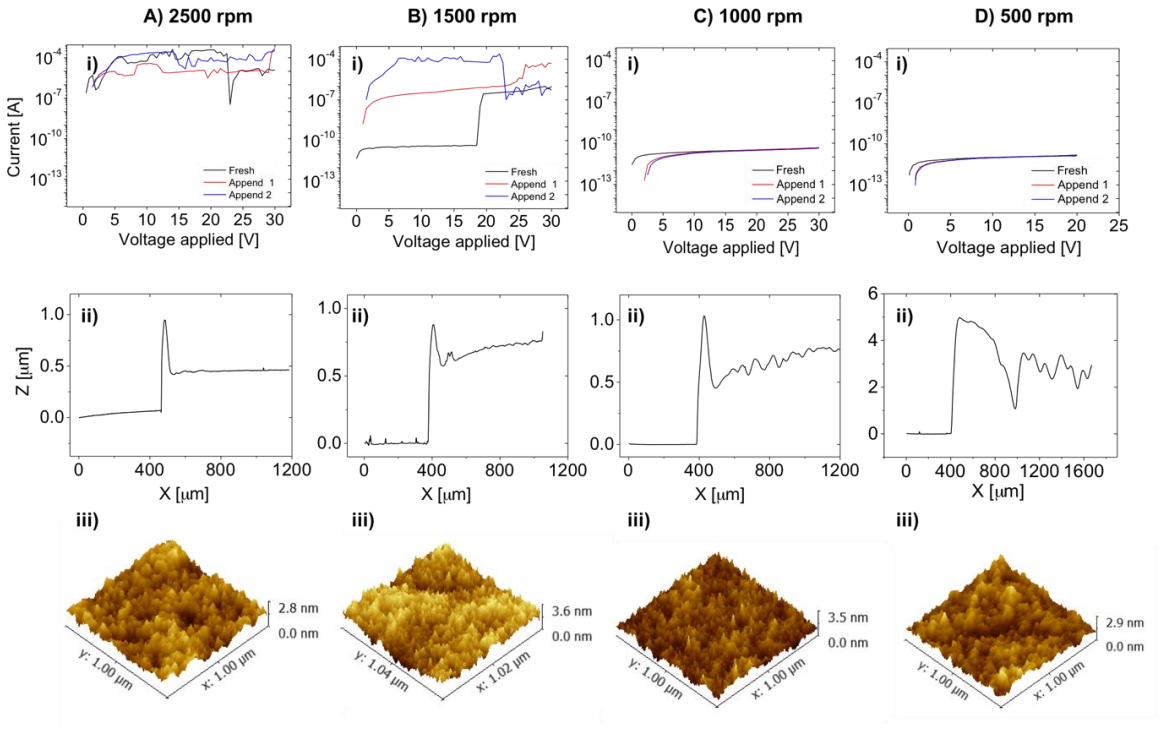

Figure 1. A), B), C), and D) show the i) leakage current of the MIE structures for a spin-coated speeds, ii) film thickness of Cytop layers, and iii) AFM topography for 2500, 1500, 1000 and 500 rpm respectively. The current-voltage curves show the current through the Cytop dielectric from three measurements.

Figure 1.ii shows the profile cross-sections of the spin-coated insulators over the metallic electrode. Although low thicknesses are desired to achieve higher capacitance values, Cytop films presented high leakage current for the MIE structures fabricated at speeds of 1500 rpm and 2500 rpm. The current through the insulator reaches values of up to 10^{-4} A. However, at lower speeds, such as at 1000 rpm and 500 rpm, leakage current is significantly minimized. The 1000 rpm MIE structures presented a current of up to $4.5*10^{-11}$ A at 30 V, which was maintained over repeated electrical measurements, while the 500 rpm structures presented the lowest leakage current of around $1.5*10^{-11}$ A. From the profilometries (Figure 1.iii), it is possible to observe a smoother surface for the 1000 rpm, 1500 rpm, and 2500 rpm layers. The morphology of the layer deposited at 500 rpm was characterized by the highest roughness because of the low speed process and the relatively high viscosity of the dielectric solution. From the Atomic Force Microscopy (AFM) analysis (see Figure 1.iii), the evaluated Root

Mean Square Roughness (RMSR) of the layers ranged between 0.4 nm and 0.5 nm. It is important to underline the absence of pinholes through the films. Table S1 (see *supporting information*) summarizes the main morphological and electrical parameters of the MIE structures. Although the lowest leakage current was obtained for the layer deposited using 500 rpm spin coating speed, its thicknesses varied in the range of microns thus preventing a good reproducibility of the insulator film. For this reason, 500 rpm was not considered for the fabrication of the BioFETs. Aiming to the accurate extraction of the capacitance of the BioFET, Electrochemical Impedance Spectroscopy (EIS) measurements were performed to the MIE structures exposed to PBS by applying a constant voltage (100mV) and sweeping the frequency over the range from 1 Hz to 1MHz. It is worth mentioning the quite high electrical capacitance in comparison with what reported in other works [23],[24],[25] in the range of 2 $\mu F*cm^{-2}$ and 2.25 $mF*cm^{-2}$ obtained for 1000 rpm and 1500 rpm, respectively at 1Hz, that will promote an optimal gate coupling. Cytop films present similar features in terms of RMS roughness and capacitance for 1500 rpm and 1000 rpm, but their leakages current differ. This disparity could arise due to slightly different profile thicknesses; there seems to be a threshold value of 0.8 μm where the dielectric is able to prevent water and ions from penetrating and diffusing into itself producing detrimental failures. As can be observed in Table S1, the yield decreases brutally from 88% to 58% when 1500 rpm is utilized and, even decay further low to 20 % for 2000 rpm. A good compromise was achieved in terms of excellent electrical insulator performance, high gate capacitance (insulator thickness), yield,and topography for the 1000 rpm layers. This spin coating speed was, thus, chosen for the further study of insulator performances.

2.3. Biofunctionalization protocol of the perfluoropolymer for BioFETs

Plenty of immobilization protocols have been developed to attach biomolecules on a wide variety of sensing layers.[26] However, the influence of these functionalization processes on

the insulating properties of organic dielectric materials is not yet well represented in the literature. For the first time, in this work, the optimization of a simple functionalization procedure that permits i) a good immobilization of the biomolecule onto the Cytop film, ii) the maintenance of the insulating properties of the Cytop preventing electrochemical reactions (such as hydrolysis), and iii) a good process yield, is presented. To this end, different functionalization parameters were considered: pH, type and concentration of the incubation buffers, dry and wet surface treatments, and the protein coupling agent. Bovine Serum Albumin (BSA) labeled with the fluorescent dye Alexa-555 was chosen as the model protein for this study. The efficiency of the immobilization process of the BSA was evaluated using fluorescence microscopy and surface modifications were checked after washing the modified surfaces. This study has been carried out directly on the MIE structures functionalized by oxygen plasma.

At first, the effect of two of the most common buffer solutions on the devices was investigated. Like PBS, 2-(N-morpholino)ethanesulfonic acid buffer (MES) is also used in the literature as a buffering agent in biology and biochemistry. It was also chosen because it is the most suitable buffer solution to stabilize (1-Ethyl-3-(3-dimethylaminopropyl)-carbodiimide)/N-hydroxysuccinimide (EDC/NHS) coupling agent. EDC/NHS chemistry was performed to assist the formation of the amide bond between the amine and carboxylic ends. EDC is a zero-length crosslinking agent commonly used to couple carboxyl or phosphate groups to primary amines and NHS was used to increase the stability of the esterification.[27],[28],[29] For both solutions, conventional pHs and concentrations were chosen (see *experimental section*). As shown in **Figure S2** (see *supporting information*), a high leakage current and poor device yield was obtained when the 100 mM MES buffer was employed (A2). This indicates that MES buffer provoked irreversible changes to the insulating polymer and should be taken out. For this reason, the same test was performed

decreasing the buffer concentration (A3, A4). Considering the results, it was clear that the 10 mM PBS (A1) and 10 mM MES (A4) buffer solutions lead to the best electrical device characteristics and they were therefore chosen for the subsequent functionalization procedures.

The different immobilization procedures used in this paper are shown in **Figure 2**.

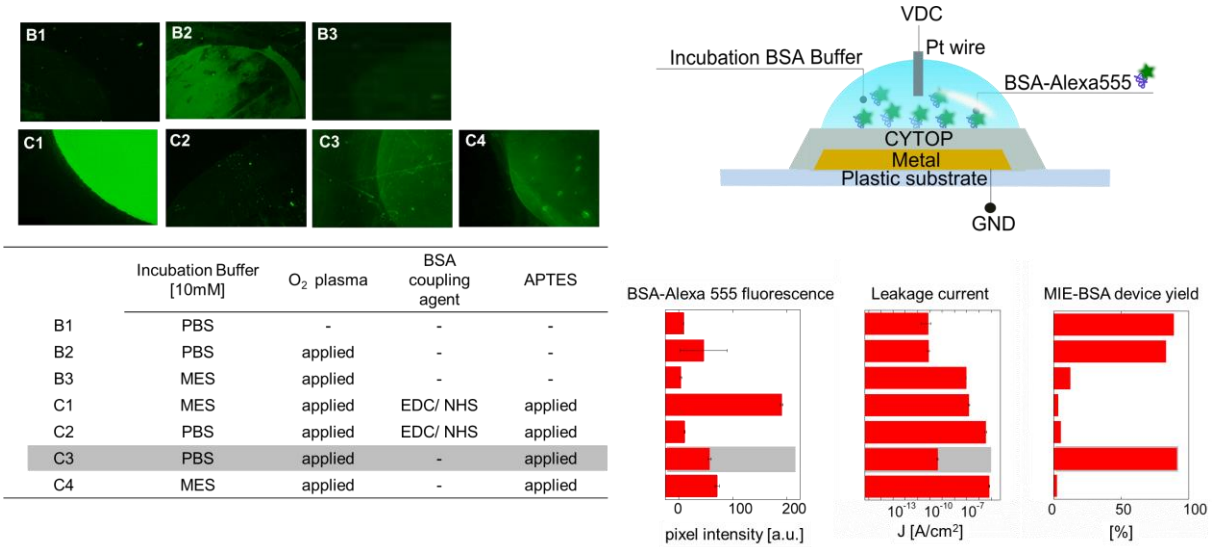

	Incubation Buffer [10mM]	O_2 plasma	BSA coupling agent	APTES
B1	PBS	-	-	-
B2	PBS	applied	-	-
B3	MES	applied	-	-
C1	MES	applied	EDC/ NHS	applied
C2	PBS	applied	EDC/ NHS	applied
C3	PBS	applied	-	applied
C4	MES	applied	-	applied

Figure 2. Scheme of the MIE structure. The protein used to study the immobilization protocol efficiency was BSA labeled with Alexa555. Fluorescence images (B1-C4) are shown for each recipe. The BSA fluorescence intensity, leakage current and MIE device yields are shown for each recipe (B1 to C4).

Initially, a control immobilization procedure based on physical absorption was considered (see Figure 2, recipe B1). As it was expected, the absence of a fluorescence signal in Figure 2-B1, clearly indicated that the protein could not be attached using electrostatic, or van der Waals interactions. This has already been observed in the literature.[30] Taking this result into account, a common oxygen plasma surface treatment was then considered. Oxygen plasma is widely used to activate organic dielectrics.[31],[32] It has been demonstrated that it can be employed to improve the binding strength and the number of the active sites available for proteins through the chemical-physical activation of oxygen functional groups on a polymer surface and by increasing its surface roughness.[33],[34] However, since plasma treatments can etch the polymer and may damage the structural properties of the sensing

devices, a 1-minute low-power plasma process was carried out (see *experimental section*). The treatment efficiency was studied using both PBS (pH 7.4) and MES (pH 5) buffers. As can be observed in recipe B2 (Figure 2), the fluorescence intensity is increased due to the attachment of the BSA onto the Cytop using PBS as the buffer and after oxygen plasma treatment. When the MES buffer is employed, the surface coverage is not homogenous probably because lower efficiency is obtained at pH 5 (Figure 2 recipe B3).

Thus, a silanization treatment was introduced to provide an amine-terminated Cytop surface onto which a covalent bond with the BSA carboxylic ends could be easily formed. The amino-(3-aminopropyl)triethoxysilane (APTES) was coupled to the organic polymer. The surface was previously activated through oxygen plasma treatment to promote the grafting of the APTES onto the insulator film.[27] The highest fluorescent intensity was achieved using the protocol based on EDC/NHS, APTES, oxygen plasma, and MES buffer (Figure 2 recipe C1). It is worth mentioning that this recipe is commonly applied to electrochemical sensors to graft biomolecules onto the surface.[27] Nevertheless, this aggressive procedure was detrimental for the Cytop layer as it produced high leakage current leading to low device yield. The same conditions were adopted replacing the MES buffer with the PBS one. This approach substantially decreased the leakage current. However, the BSA immobilization was reduced because the EDC/NHS reaction performs better at pH 5 (Figure 2 recipe C2).[35] Less immobilization efficiency was achieved when the EDC/NHS was removed from the protocol (Figure 2 recipe C3 and recipe C4). High leakage current persisted when MES was used as the incubation buffer. The best compromise in terms of BSA immobilization efficiency, leakage current, and device yield was obtained for the amine-functionalized Cytop surface performed in PBS buffer without EDC/NHS chemistry (Figure 2 recipe C3). Therefore, the recipe C3 will be employed for the immobilization protocol of the antibodies in the BioFET device.

As a further demonstration of the effectiveness of the proposed protocol, a quantitative analysis was undertaken. The effect of the oxygen plasma treatment and the attachment of the APTES molecules onto the Cytop surfaces were confirmed by contact angle, AFM, and X-ray Photoemission Spectroscopy (XPS) analysis. As can be seen in **Figure S3**.A (see *supporting information*), the contact angle decreases from 110º for untreated Cytop films to 47º upon plasma oxidation of the surface. The decrease in the hydrophobicity of the organic insulator is the consequence of the increase in the density of the oxygen-related moieties on its surface. The expected increase of the contact angle to 107º observed in the APTES treated insulator is in concordance with what is usually observed in amine-terminated surfaces.[7],[36] After the washing step to remove the excess of non-attached APTES, the same contact angle value was measured, indicating a good surface functionalization. **Figure S4** (see *supporting information*) depicts the XPS spectra from the Cytop surface before (i) and after (ii) the functionalization procedure. The F1s peak appears in both spectra at around 689 eV, the energy value typical of organic fluorine and already reported for Cytop.[37] Upon APTES functionalization of the Cytop layer, nitrogen and silicon peaks appear on the XPS spectrum (Figure S4.ii and upper-left and upper-right insets in *supporting information*). These confirm APTES conjugation to the Cytop surface since APTES contains both a terminal amino group and a terminal silicon group which are not present in the bare Cytop, as indicated in Figure S4.i (see *supporting information*) and in Figure S1, respectively. The nitrogen peak at around 400 eV can be attributed to the APTES terminal amino group, which at the pH =7.4 utilized in this study, may exist in three different forms (NH_3^+, hydrogen-bonded NH_2 group NH_2-H, and free NH_2), as already observed elsewhere.[38] Figure S4.B (see *supporting information*) shows a broad C1s peak centered at around 290 eV that can be easily attributed to the different C-F bonds of the Cytop molecule;[39],[40] while the C1s

peak at 285 eV, shown in the upper central inset in Figure S4.B (see *supporting information*), is typical of the C-C alkyl chain that is present in APTES but not in Cytop.[41]

2.4. Top-gate organic BioFETs fabricated with conventional techniques

In order to demonstrate the actual feasibility of the OFETs to work in aqueous conditions, top-gate bottom-contact BioFETs have been fabricated, using thermally evaporated gold as drain and source electrodes and, spin-coated amorphous OSC; details are reported in the *experimental section*. **Figure 3**A and Figure 3B show an optical image and the structure scheme. The device performances of top-gate BioFETs were investigated. Figure 3C, Figure 3D and Figure 3E display a typical transfer characteristic in logarithmic and linear scale, and an output characteristic of non-functionalized top-gate BioFETs in aqueous media, respectively. It is important to highlight that all the non-functionalized BioFETs presented negligible electrical hysteresis behavior, 15 mV at worst, and operated at voltages lower than 10 V. Furthermore, as a remarkable achievement in this work, the leakage current of the BioFETs was extremely low, in the range of tens of picoampers. The transfer characteristics were recorded using a sweeping rate of 1.2 V/s which corresponds to a frequency of ~1Hz, the same used for the capacitance measurements reported in Table S1. Considering this value (2 $\mu F/cm^2$), the maximum field-effect mobility and I_{ON}/I_{OFF} ratio were $10 \cdot 10^{-3}$ $cm^2/V*s$ and 10^3, respectively. All the devices worked in enhancement mode, with threshold voltage values between -1.46 V and -2.04 V. **Table S2** summarizes the main top-gate BioFET electrical parameters (see *supporting information*). The overall performances of the devices reported here are very promising as a good yield process was obtained thereby assuring a proper fabrication procedure that will enable a scalable production. Lower operation voltages could be achieved using crystalline OSCs with higher mobility. However, the occurrence of crystallization phenomenon is not suitable for top-gate configurations.

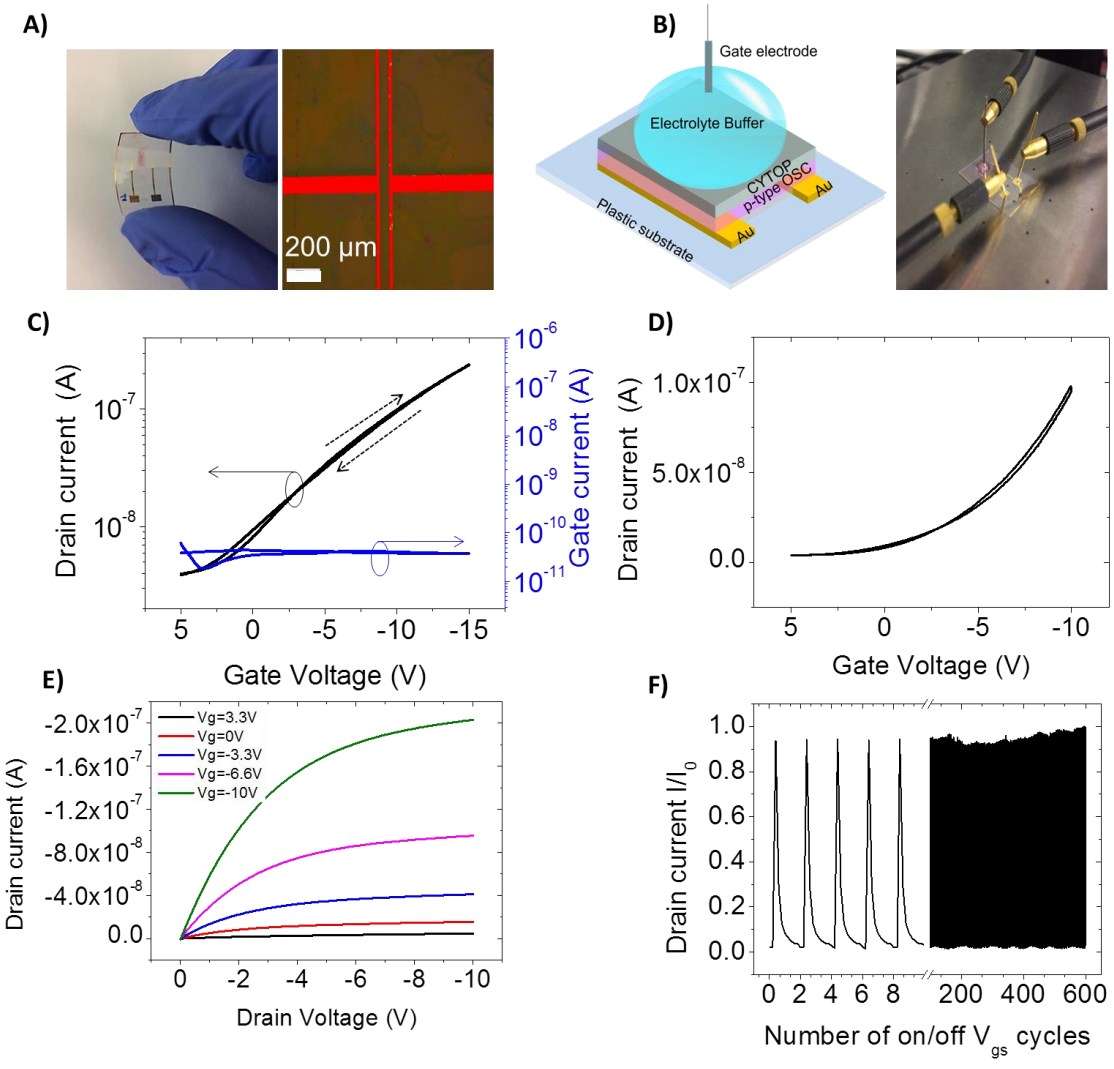

Figure 3. A) Optical image of the fabricated top-gate BioFET. The zoom shows the channel of the BioFET. B) Scheme and optical image of the electrical characterization set-up of the top-gate BioFETs. C) I_{DS}-V_{GS} and I_{GS}-V_{GS} curves of top-gate BioFET in logarithmic scale, D) I_{DS}-V_{GS} curve of top-gate BioFET in linear scale, E) Output characteristic for top-gate BioFET and F) I_{DS} vs V_{GS} (-5V to 0V) at V_{DS} (-5V) measured up to 600 cycles. A frequency of 1Hz was employed. All the electrical characteristics were measured under a 10 µL PBS droplet placed over the Cytop layer.

In addition to the static electrical characteristics, operational stability over several cycles was evaluated to confirm the possibility of using our BioFET structure as an actual sensor where several read-outs would be needed. Specifically, this dynamic test was carried out to reveal the time response of the BioFETs and to evaluate its possible degradation over time. It is known that water molecules can create deep traps under continuous bias stress.[23] Figure 3F

shows a cyclic test where the BioFET was subjected to several on and off gate voltage cycles at constant drain voltage. The gate polarization was varied between -5V (on-state) and 0V (off-state) over 600 cycles. The drain current did not deviate, thus demonstrating the outstanding operational stability of top-gate BioFETs in aqueous media.

The immobilization of anti-human IgG (αHIgG) model antibody was first studied to evaluate the potential of the BioFETs as immunosensing platforms. αHIgG protein was immobilized onto the amine-functionalized Cytop insulator through peptide bonds (see *experimental section* and **Figure S5**) and its presence on the BioFET was monitored through changes in the drain current. Further details can be found in the section *Electrical characterization of the BioFET under immobilization protocol* and **Figure S6** in *supporting information*.

2.5. Top-gate organic BioFETs fabricated with printing technique

Once the functionalization procedure of the organic dielectric was assessed, and an unambiguous demonstration of its actual feasibility for the fabrication of BioFETs was given, inkjet-printed BioFETs have been fabricated. The main difference is that the drain and source electrodes and the OSC were deposited by inkjet-printing technique (see **Figure S7**). The drain and source electrodes were inkjet-printed using a novel Au ink which allows a good alignment among the Work Function (WF) of the OSC and the electrodes and, at the same time, decreases the cost and the time of the device fabrication in comparison with conventional evaporation techniques. The printing parameters of the Au electrodes were optimized to have the same thickness than the evaporated ones, ranging from 140 to 167 nm, and most conductive electrodes (44 Ω/square) as possible. **Figure S8.A** and Figure S8.B show profilometric and Scanning Electronic Microscope (SEM) analysis of the microscale features of the inkjet-printed Au electrode. The printed devices present a channel length of 38±7 μm. Once the printing procedure of thin electrodes was assessed, the OSC was

patterned into the channel by inkjet-printing. Also, in this case, a thin layer is desired.[18] Since the BioFET is a stack of thin film layers, the morphology of the OSC is paramount in order to achieve a high quality OSC/dielectric interface. Inkjet-printed small molecule OSC films present large surface roughness, due to grain boundary typical of polycrystalline materials, that can be detrimental for the good deposition of the insulator layer on top.[42] Thus, an amorphous OSC was chosen. As can be observed from SEM and Atomic Force Microscopy (AFM) analysis the inkjet-printed OSC film showed a good uniformity (roughness of 6.95 nm) but some agglomeration typical of polymers are visible in Figure S8.C and Figure S8.D, respectively. The profile thickness of the inkjet-printed OSC films ranges from 90 to 100 nm.

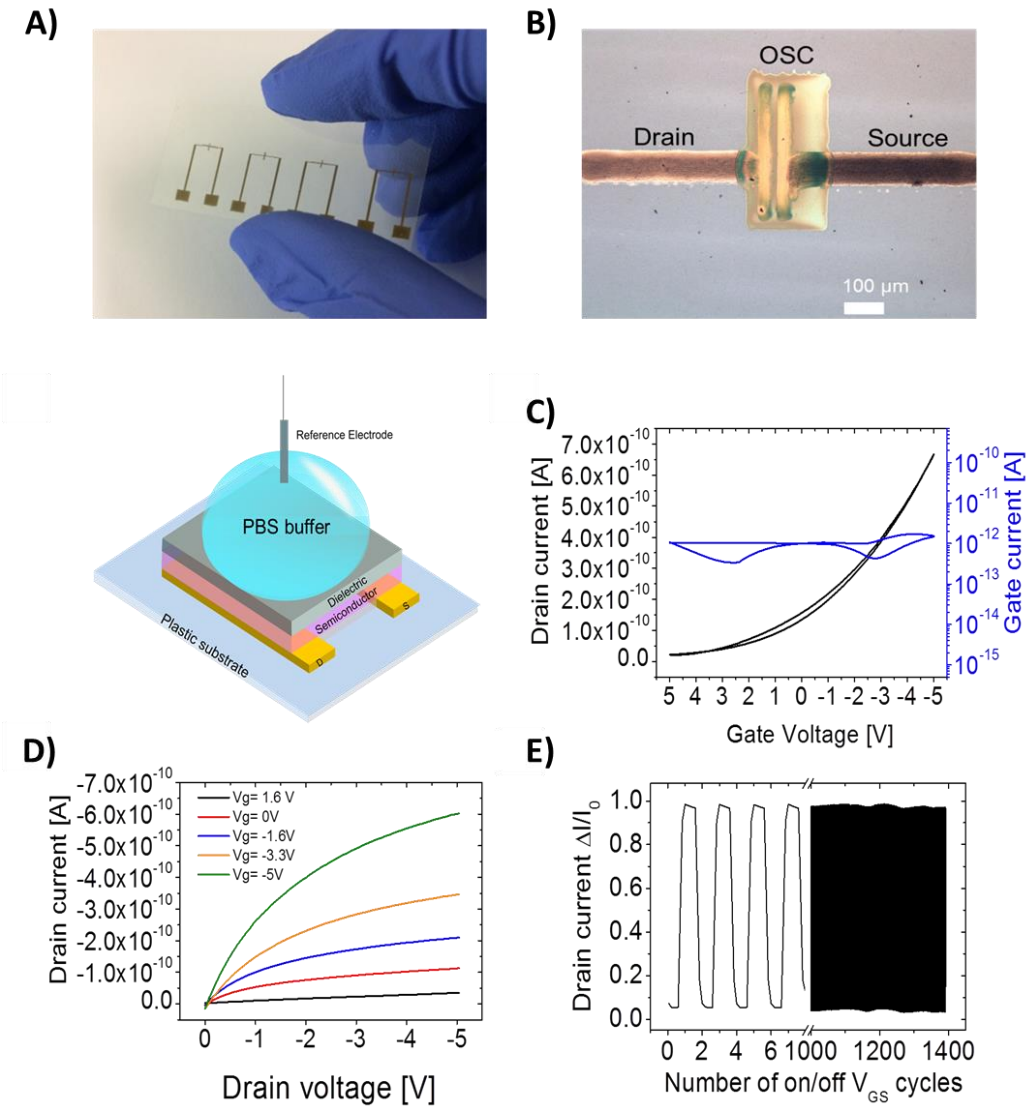

Figure 4. A) Optical image of the fabricated top-gate inkjet-printed BioFET. B) Optical image of the channel of the inkjet-printed BioFET and scheme of the electrical characterization set-up of the top-gate BioFETs. C) I_{DS}-V_{GS} and I_{GS}-V_{GS} curves of top-gate inkjet-printed BioFET. D) Output characteristic for top-gate BioFET and E) I_{DS} vs V_{GS} (-5V to 0V) at V_{DS} (-5V) measured up to 1400 cycles. All the electrical characteristics were measured under a 10 µL PBS droplet placed over the Cytop layer.

Figure 4.A and **Figure 4.B** show an optical image of the inkjet-printed gold electrodes and the BioFET device, respectively. The device performances of top-gate BioFETs were investigated. Figure 4C, Figure 4D and Figure 4E display the transfer, and output characteristics of non-functionalized top-gate inkjet-printed BioFETs in aqueous media, respectively. In particular, transfer curve and output curve were recorded until -5 V to prove that the BioFETs can be modulated at significant low voltages. It is important to highlight that all the non-functionalized inkjet-printed BioFETs presented near hysteresis-free

electrical behaviors, 870 mV at worst. Moreover, as a remarkable achievement in these inkjet-printed devices, the leakage current of the BioFETs was extremely low, in the range of picoampers at -5V. Assuming the values of the capacitance at 1 Hz, the average field-effect mobility and I_{ON}/I_{OFF} ratio were $1 \cdot 10^{-5}$ $cm^2/V \cdot s$ and 70, respectively. All the devices worked in enhancement mode, with threshold voltage values of -0.5 V. Table S3 summarizes the main top-gate inkjet-printed BioFET electrical parameters (see *supporting information*).

2.6. Immunosensor for human IgG (HIgG) detection

BioFETs potential as immunosensing platforms was evaluated through their ability for the immobilization of anti-human IgG (αHIgG) model antibody, and the specific detection of human IgG (HIgG) antigen. αHIgG antibody was firstly immobilized onto the amine-functionalized Cytop insulator through peptide bonds (**Figure 5.A**), as previously optimized for BSA (recipe C3). The αHIgG concentration was fixed at 400 µg mL^{-1} and non-specific absorptions were avoided by blocking the BioFET surface with casein before the incubation of the antigen.[43] The immunocomplex formation with HIgG was monitored through drain current measurements of the transfer characteristics. The Isoelectric Point (pI) of the HIgG is about 6.6-8.5[44] what means that it is negatively charged at the pH of the working buffer (pH 9), so an increase in the current is expected for an increase of the antigen concentration. It is possible to presume that the negative charges of the HIgG attract the holes to the transistor channel region increasing the overall current. **Figure S9** shows source-drain current- gate voltage characteristics for the BioFET in contact with solutions containing the antigen HIgG in different concentrations, ranging from pure PBS (called as blank in Figure S9) to 500 µg mL^{-1}. For a given gate voltage, fixed at V_G=-5V, a quantitative analysis of the drain current variation as function of the HIgG concentration is reported in Figure 5.B.

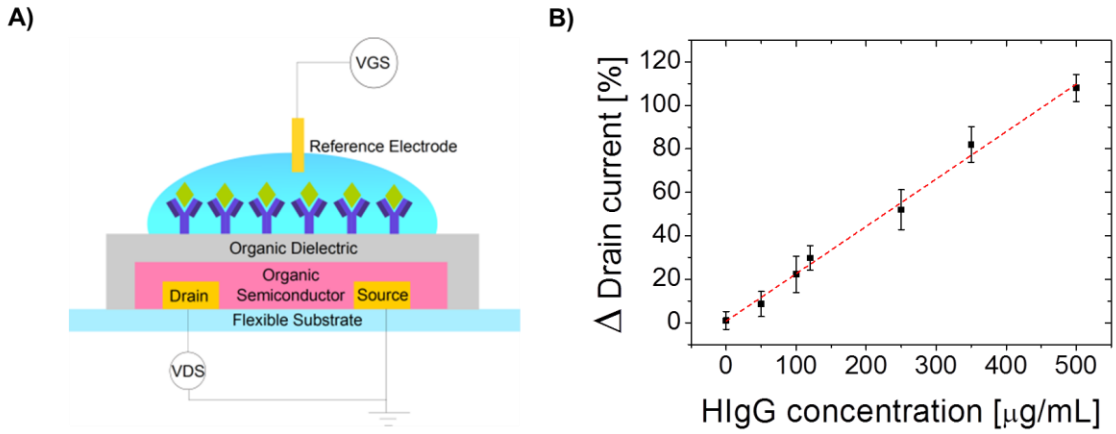

Figure 5. A) Schematic of the BioFET immunosensor performed by immobilizing **α**HIgG antibodies onto amine-functionalized Cytop and detecting HIgG antigen by measuring changes in drain current. B) Percentage of the change of the drain current (I_{DS}) from functionalized top-gate BioFET as function of HIgG antigen concentration.

The analysis of the results indicates that the current increases when the antigen is specifically linked to the amine-functionalized Cytop film through the immunoreaction, as expected. A linear plot is obtained when relating the percentage change of the drain current with analyte HIgG concentration, the fitting function of the curve is $\Delta I_{DS}/I_{DS}(\%) = 0.21c + 3.04$ (where c is the HIgG concentration) with an R^2 of 0.994. The method shows a reproducibility in terms of relative standard deviation (RSD) of 12% (n=3) for a HIgG concentration of 250 □g mL^{-1}. The limit of detection (LOD) of the method, estimated as three times the standard deviation divided by the slope of the calibration curve is 5.71 μg mL^{-1}. More detailed studies on these transistors could be carried out for a specific antibody. In particular, the BioFET could be applied to applications such as gene therapy, antibody response to vaccines or development of antibodies with cytotoxicity to cancer cells among others.[45],[46] The LOD value of the BioFET can be explained through the device architecture, technology and materials employed. Higher LOD can be obtained using organic semiconductors and organic dielectrics with higher carrier mobility and dielectric constant, respectively. The specificity of the immunosensor was demonstrated by assaying a nonspecific antigen (goat IgG) instead of

HIgG, which did not gave significative changes in the drain current measured, as shown in Figure S6 at the *supporting information*. The analysis of the biosensors using other antibody-antigen complexes and the use of complex matrixes to study the specificity under real samples are beyond the scope of this work. Further optimizations about detection limit will be examined as future work. Moreover, the sensing evaluation performed in this work has to be considered as a promising proof-of-concept.

It is worth mentioning there has not been much scientific contribution related to dielectric layers for top gated biomolecule sensors thus, it remains desirable to reinforce them. Regarding to this lack, our contribution is significant since it is the first work, to the best of our knowledge, that makes feasible the realization of these devices using flexible substrates, low-cost fabrication techniques and, organic materials, especially hydrophobic polymers. For comparison purposes, **Table S4** shows previous works related to the development of organic thin film transistors using hydrofobic dielectric layers for top gated biomolecule sensors.

3. Conclusions

In this work, a systematic study on the development of novel top-gate inkjet-printed BioFETs is presented. An exhaustive electrical and morphological investigation on different gate insulators was carried out and Cytop was selected for its remarkable insulating properties. The Cytop film was optimized in terms of film thickness and leakage current and an amine-terminated Cytop surface was obtained via a silanization reaction with APTES, onto which the immobilization of biomolecules was investigated. Good BioFET performances have been demonstrated using the Cytop as gate dielectric over thermally evaporated devices. In as second phase, inkjet-printed BioFETs were developed for the achievement of low-cost devices. The patterning of the drain and source electrodes was carried out using a novel Au nanoparticle ink. The inkjet-printed BioFET demonstrated to detect the HIgG with a LOD of

5.71 μg mL^{-1}, with good reproducibility and selectivity. It is expected that this novel BioFET device will make an important contribution to the development of new top-gate BioFETs for immunosensing applications.

4. Experimental Section

MIE fabrication: MIE devices were fabricated on 125 μm thick Polyethylene-2,6-napthalene (PEN) Teonex Q65HA substrates from Dupont Teijin specially developed for flexible electronics. After cleaning with organic solvents, the metallic bottom electrode was patterned using a Dimatix Materials Printer DMP 2831 (FujiFilm) under ambient conditions. In order to improve adhesion and the wettability of the printed layer, oxygen plasma was carried out using a microwave plasma generator (Smart Plasma system, Plasma Technology GmbH). The condition used was 40W plasma power for 20 sec. A gold nanoparticle-based ink based on aqueous solution was employed (DryCure JB, Colloidal-ink Company). The ink was deposited using a single drop volume of 10pL with a cartridge temperature of 35ºC. A drop spacing of 25 μm was used, employing one nozzle and using a printer platen temperature of 45ºC. The printed layer was annealed in a hotplate for 45 min at 120ºC in order to remove the solvent and sinter the gold ink. Separate depositions of cPVP, SU-8, PMMA and Cytop were carried out as follows. The cPVP was prepared by dissolving PVP in PGMEA at room temperature and the resulting solution was stirred for 30 min. The deposition was carried out by spin coating at 1000 rpm for 30 sec and the resulting layer was then cured at 150 °C for 20 min. The SU-8 was spin-coated at 3000 rpm for 20 sec. and at 5000 rpm for 20 sec and then cured at 95 ºC for 30 min and 1 min under UV-source. The PMMA was deposited by spin-coating at 1500 rpm for 30 sec. onto the metallic electrode, and then cured at 150 °C for 90 sec. on a hot plate. The Cytop solution (CTL-809M with a concentration of 9%, Asahi Glass), without further dilution, was deposited by spin-coating at 1000 rpm for 30 sec. and then cured on a hot plate at 100 ºC for 120 min.

Top-gate BioFET fabrication: Flexible bottom-gate BioFETs were fabricated on 125 μm thick Poly/ethylene-2,6-napthalene dicarboxylate (PEN) Teonex Q65FA substrates from Dupont Teijin specially developed for flexible electronics. After cleaning with organic solvents, the drain and source electrodes had been patterned in two different ways. Initially, titanium (Ti) and gold (Au) source and drain electrodes (100 nm thick) were thermally evaporated through a shadow mask having a channel width (W) of 1.5 mm and length (L) of 60 μm. In inkjet-printed devices, the drain and source electrodes were patterned using a Dimatix Materials Printer 2831 (FujiFilm) under ambient conditions. In order to improve adhesion and the wettability of the printed layer, oxygen plasma was carried out using a microwave plasma generator (Smart Plasma system, Plasma Technology GmH). The condition used was 40W plasma power for 20 sec. A gold nanoparticle-based ink based on aqueous solution was employed (DryCure JB, Colloidal-ink Company). The ink was deposited using a single drop volume of 10 pL with a cartridge temperature of 35 ºC in order to reach high resolution. A drop spacing of 25 μm was used, employing one nozzle and using a printer platen temperature of 45ºC. The printed layer was annealed in a hotplate for 45 min at 120 ºC in order to remove the solvent and sinter the gold ink. Afterwards, the p-type SP400-1750 amorphous OSC dissolved in mesitylene and 1-methylnaphthalene from Merck Chemicals had been deposited in two different ways. Initially, the OSC was spin-coated at 500 rpm for 15 sec. and after at 1500 rpm for 120 sec. and the solvent was removed by thermal annealing on a hot plate at 100 ºC for 120 sec. In inkjet-printed devices, the OSC was patterned using inkjet-printing technique. The ink was deposited using a single drop volume of 10 pL with a cartridge at room temperature. A drop spacing of 15 μm was used, employing one nozzle in order to obtain a thin film. During the deposition, the printed platen was kept at room temperature. The printed layer was annealed in a hotplate for 2 min at 100 ºC. Finally, the OSC layer was covered with Cytop solution (CTL-809M with a concentration of 9%,

Asahi Glass), without further dilution, and was deposited by spin-coating at 1000 rpm for 30 sec. and then cured on a hot plate at 100 ºC for 120 min.

Surface functionalization of the Cytop: oxygen plasma was carried out using a microwave plasma generator (Smart Plasma system, Plasma Technology GmH). The condition used was 40W plasma power for 60 sec. Anhydrous 3-aminopropyltriethoxysilane (APTES, 99%) was purchased from Sigma Aldrich and used as received. The hydrolyzed APTES solution was obtained by mixing 95 mM of absolute ethanol and 5 mL of deionized water, and by adding drop by drop 5 mL of APTES under continual stirring. The top-gate BioFETs were immersed in this solution for 120 min. at room temperature, followed by thorough rinsing with ethanol to remove any excess reagent. Finally, the APTES-modified Cytop was heated in a hot plate at 100 ºC for 120 min. and then stored in a desiccator under vacuum until further use. Phosphate buffer saline, MES buffer and EDC/NHS were obtained from Sigma Aldrich. Bovine serum albumin (BSA) labeled with Alexa Fluor 555 dissolved in PBS was acquired from Thermofisher.

Electrical characterization: A Pt wire immersed in the electrolyte was used to modulate the channel conductivity by a applying a voltage between the electrode and the bottom contact for MIE and drain/source for BioFETs. All the electrical measurements were carried out using an Agilent B1500A Semiconductor Analyzer with a sweep rate of 1.2 V/s and a current compliance of 1mA. For all the devices, the mobility and the threshold voltages were estimated from the slope of the square of the drain current versus V_G. All the measurements were performed in ambient conditions.

Surface characterization: The layer thicknesses for the dielectric layers were evaluated using a mechanical surface Dektak profilometer. The optical images were acquired using a light microscope DM4000 from Leica. Atomic Force Microscopy images were carried out using a

Nanoscope Veeco Dimension 3100. Scanning Electronic Microscope images were performed using a E beam SEM Zeiss Leo 1530. X-ray photoelectron spectroscopy (XPS) analysis was performed in an ultrahigh vacuum apparatus built by SPECS Phoibos 150. The surface wettability was also performed using a contact angle analyzer. Measurements were performed at room temperature under open-air conditions using a DSA 100 contact angle measuring device (Krüss, Germany). Static contact angles were measured using the sessile droplet method.

Antibody immobilization and antigen detection: anti-Human IgG (anti-HIgG, ref. I1886; polyclonal antibody developed in goat), Human IgG (HIgG, ref. I2511) and goat IgG (GIgG, ref. I5256) were purchased from Sigma. The capture antibody was immobilized on the amine-functionalizated Cytop by dropping 20 µL of αHIgG solution at different concentrations prepared in 0.001 M PBS buffer of pH 7.4 and incubating during 90 min at room temperature in a humid ambient chamber. A washing step with 0.001 M PBS solution was then carried out. Subsequently, 20 µL of 0.5% casein (w/v) prepared in 0.001 M PBS buffer of pH7.4 were used to block the possible active binding sites on the BioFET surface. After 60 min incubation at room temperature and further washing with 0.001 M PBS buffer (pH7.4), the immunoreaction was performed by placing 20 µL of a 400 µg mL^{-1} solution of HIgG and leaving for 90 min at room temperature. Finally, the BioFET was rinsed with 0.001 M PBS buffer (pH 7.4) to remove unbounded HIgG prior to the electrical measurements. The same experimental procedure was followed for the control assays, performed with GIgG instead of HIgG.

Acknowledgements

We acknowledge support from the Spanish MINECO under project MAT2017-87202-P. ICN2 is supported by the Severo Ochoa program from Spanish MINECO (Grant no. SEV-2013-0295) and by the CERCA Programme/Generalitat de Catalunya. This work was also partly supported by the Catalan Government (Grant 2017-SGR-1624), the Spanish MINECO (projects RTC-2015-4184-1) and MICIU (project RTI2018-102070-B-C21) and it has been done in the framework of PhD Programme in Electrical and Telecommunication Engineering of Universitat Autònoma de Barcelona (UAB). The authors would like to thank our R&D partners: Fujifilm Dimatix, Ceradrop and DuPont Teijin for providing us with the research related consumables and their technical details. Finally, the authors wish to thank Merck Chemicals (UK) and Asahi Glass (Japan) for providing the organic semiconductor ink and the Cytop dielectric solution.

References

[1] W.L. Kalb, T. Mathis, S. Haas, A.F. Stassen, B. Batlogg, Organic small molecule field-effect transistors with Cytop^{TM} gate dielectric: Eliminating gate bias stress effects, Appl. Phys. Lett. 90 (2007) 092104. https://doi.org/10.1063/1.2709894.

[2] X. Cheng, M. Caironi, Y.-Y. Noh, J. Wang, C. Newman, H. Yan, A. Facchetti, H. Sirringhaus, Air Stable Cross-Linked Cytop Ultrathin Gate Dielectric for High Yield Low-Voltage Top-Gate Organic Field-Effect Transistors, Chem. Mater. 22 (2010) 1559–1566. https://doi.org/10.1021/cm902929b.

[3] M.P. Walser, W.L. Kalb, T. Mathis, B. Batlogg, Low-voltage organic transistors and inverters with ultrathin fluoropolymer gate dielectric, Appl. Phys. Lett. 95 (2009) 233301. https://doi.org/10.1063/1.3267055.

[4] B.-J. de Gans, P.C. Duineveld, U.S. Schubert, Inkjet Printing of Polymers: State of the Art and Future Developments, Adv. Mater. 16 (2004) 203–213. https://doi.org/10.1002/adma.200300385.

[5] A. Teichler, J. Perelaer, U.S. Schubert, Inkjet printing of organic electronics-comparison of deposition techniques and state-of-the-art developments, J. Mater. Chem. C. 1 (2013) 1910–1925. https://doi.org/10.1039/c2tc00255h.

[6] T. Cramer, A. Campana, F. Leonardi, S. Casalini, A. Kyndiah, M. Murgia, F. Biscarini, Water-gated organic field effect transistors – opportunities for biochemical sensing and extracellular signal transduction, J. Mater. Chem. B. 1 (2013) 3728. https://doi.org/10.1039/c3tb20340a.

[7] F. Buth, A. Donner, M. Sachsenhauser, M. Stutzmann, J.A. Garrido, Biofunctional electrolyte-gated organic field-effect transistors, Adv. Mater. 24 (2012) 4511–4517. https://doi.org/10.1002/adma.201201841.

[8] W. Guan, M.A. Reed, Biosensors and Biodetection, Humana Press, Totowa, NJ, 2009. https://doi.org/10.1007/978-1-60327-569-9.

[9] D.K. Hwang, C. Fuentes-Hernandez, J. Kim, W.J. Potscavage, S.-J. Kim, B. Kippelen, Top-Gate Organic Field-Effect Transistors with High Environmental and Operational Stability, Adv. Mater. 23 (2011) 1293–1298. https://doi.org/10.1002/adma.201004278.

[10] H.U. Khan, J. Jang, J.-J. Kim, W. Knoll, Effect of passivation on the sensitivity and stability of pentacene transistor sensors in aqueous media, Biosens. Bioelectron. 26 (2011) 4217–4221. https://doi.org/10.1016/j.bios.2011.03.031.

[11] T.-J. Ha, D. Kiriya, K. Chen, A. Javey, Highly Stable Hysteresis-Free Carbon Nanotube Thin-Film Transistors by Fluorocarbon Polymer Encapsulation, ACS Appl.

Mater. Interfaces. 6 (2014) 8441–8446. https://doi.org/10.1021/am5013326.

[12] A. Benor, J.E. Northrup, A. Hoppe, V. Wagner, D. Knipp, Electrical and environmental stability of organic transistors, (2015) 108–131. https://doi.org/10.7567/ssdm.2009.f-2-1.

[13] H. Sirringhaus, Reliability of Organic Field-Effect Transistors, Adv. Mater. 21 (2009) 3859–3873. https://doi.org/10.1002/adma.200901136.

[14] S.H. Han, J.H. Kim, J. Jang, S.M. Cho, M.H. Oh, S.H. Lee, D.J. Choo, Lifetime of organic thin-film transistors with organic passivation layers, Appl. Phys. Lett. 88 (2006) 073519. https://doi.org/10.1063/1.2174876.

[15] S. Lee, J.-S. Park, T.R. Lee, The Wettability of Fluoropolymer Surfaces: Influence of Surface Dipoles, Langmuir. 24 (2008) 4817–4826. https://doi.org/10.1021/la700902h.

[16] W. Huang, K. Besar, R. LeCover, P. Dulloor, J. Sinha, J.F. Martínez Hardigree, C. Pick, J. Swavola, A.D. Everett, J. Frechette, M. Bevan, H.E. Katz, Label-free brain injury biomarker detection based on highly sensitive large area organic thin film transistor with hybrid coupling layer, Chem. Sci. 5 (2014) 416–426. https://doi.org/10.1039/C3SC52638K.

[17] M.E. Roberts, N. Queraltó, S.C.B. Mannsfeld, B.N. Reinecke, W. Knoll, Z. Bao, Cross-Linked Polymer Gate Dielectric Films for Low-Voltage Organic Transistors, Chem. Mater. 21 (2009) 2292–2299. https://doi.org/10.1021/cm900637p.

[18] K. Fukuda, Y. Takeda, M. Mizukami, D. Kumaki, S. Tokito, Fully Solution-Processed Flexible Organic Thin Film Transistor Arrays with High Mobility and Exceptional Uniformity, Sci. Rep. 4 (2015) 3947. https://doi.org/10.1038/srep03947.

[19] C.H. Kim, D. Tondelier, B. Geffroy, Y. Bonnassieux, G. Horowitz, Characterization of

the pentacene thin-film transistors with an epoxy resin-based polymeric gate insulator, Eur. Phys. J. Appl. Phys. 57 (2012) 20201. https://doi.org/10.1051/epjap/2011110272.

[20] K. Tetzner, I. Bose, K. Bock, Organic Field-Effect Transistors Based on a Liquid-Crystalline Polymeric Semiconductor using SU-8 Gate Dielectrics onFlexible Substrates, Materials (Basel). 7 (2014) 7226–7242. https://doi.org/10.3390/ma7117226.

[21] T.-S. Huang, Y.-K. Su, P.-C. Wang, Poly(methyl methacrylate) Dielectric Material Applied in Organic Thin Film Transistors, Jpn. J. Appl. Phys. 47 (2008) 3185–3188. https://doi.org/10.1143/JJAP.47.3185.

[22] M. Ieda, Dielectric Breakdown Process of Polymers, IEEE Trans. Electr. Insul. EI-15 (1980) 206–224. https://doi.org/10.1109/TEI.1980.298314.

[23] D.K. Hwang, C. Fuentes-Hernandez, M. Fenoll, M. Yun, J. Park, J.W. Shim, K.A. Knauer, A. Dindar, H. Kim, Y. Kim, J. Kim, H. Cheun, M.M. Payne, S. Graham, S. Im, J.E. Anthony, B. Kippelen, Systematic Reliability Study of Top-Gate p- and n-Channel Organic Field-Effect Transistors, ACS Appl. Mater. Interfaces. 6 (2014) 3378–3386. https://doi.org/10.1021/am405424k.

[24] G. Yoo, S.L. Choi, S. Lee, B. Yoo, S. Kim, M.S. Oh, Enhancement-mode operation of multilayer MoS 2 transistors with a fluoropolymer gate dielectric layer, Appl. Phys. Lett. 108 (2016) 263106. https://doi.org/10.1063/1.4955024.

[25] S.H.H. Shokouh, P.J. Jeon, A. Pezeshki, K. Choi, H.S. Lee, J.S. Kim, E.Y. Park, S. Im, High-Performance, Air-Stable, Top-Gate, p-Channel WSe 2 Field-Effect Transistor with Fluoropolymer Buffer Layer, Adv. Funct. Mater. 25 (2015) 7208–7214. https://doi.org/10.1002/adfm.201502008.

[26] D. Kim, A.E. Herr, Protein immobilization techniques for microfluidic assays, Biomicrofluidics. 7 (2013) 1–47. https://doi.org/10.1063/1.4816934.

[27] S.K. Vashist, E. Lam, S. Hrapovic, K.B. Male, J.H.T. Luong, Immobilization of Antibodies and Enzymes on 3-Aminopropyltriethoxysilane-Functionalized Bioanalytical Platforms for Biosensors and Diagnostics, Chem. Rev. 114 (2014) 11083–11130. https://doi.org/10.1021/cr5000943.

[28] M.J.E. Fischer, Amine Coupling Through EDC/NHS: A Practical Approach, in: Mol. Biomethods Handb. Second Ed., 2010: pp. 55–73. https://doi.org/10.1007/978-1-60761-670-2_3.

[29] C.K. Dixit, S.K. Vashist, B.D. MacCraith, R. O'Kennedy, Multisubstrate-compatible ELISA procedures for rapid and high-sensitivity immunoassays, Nat. Protoc. 6 (2011) 439–445. https://doi.org/10.1038/nprot.2011.304.

[30] J. Choi, H.G. Jeon, O.E. Kwon, I. Bae, J. Cho, Y. Kim, B. Park, Improved output characteristics of organic thin film transistors by using an insulator/protein overlayer and their applications, J. Mater. Chem. C. 3 (2015) 2603–2613. https://doi.org/10.1039/c4tc02823f.

[31] I.A. Grimaldi, G. Testa, G. Persichetti, F. Loffredo, F. Villani, R. Bernini, Plasma functionalization procedure for antibody immobilization for SU-8 based sensor, Biosens. Bioelectron. 86 (2016) 827–833. https://doi.org/10.1016/j.bios.2016.07.090.

[32] R. Landgraf, M.K. Kaiser, J. Posseckardt, B. Adolphi, W.J. Fischer, Functionalization of Polymer Sensor Surfaces by Oxygen Plasma Treatment, Procedia Chem. 1 (2009) 1015–1018. https://doi.org/10.1016/j.proche.2009.07.253.

[33] Y. Yuan, H. He, L.J. Lee, Protein a-based antibody immobilization onto polymeric

microdevices for enhanced sensitivity of enzyme-linked immunosorbent assay, Biotechnol. Bioeng. 102 (2009) 891–901. https://doi.org/10.1002/bit.22136.

[34] M.M. Bilek, D.R. McKenzie, Plasma modified surfaces for covalent immobilization of functional biomolecules in the absence of chemical linkers: towards better biosensors and a new generation of medical implants, Biophys. Rev. 2 (2010) 55–65. https://doi.org/10.1007/s12551-010-0028-1.

[35] N. Nakajima, Y. Ikada, Mechanism of Amide Formation by Carbodiimide for Bioconjugation in Aqueous Media, Bioconjug. Chem. 6 (1995) 123–130. https://doi.org/10.1021/bc00031a015.

[36] L. Tang, N.Y. Lee, A facile route for irreversible bonding of plastic-PDMS hybrid microdevices at room temperature, Lab Chip. 10 (2010) 1274–1280. https://doi.org/10.1039/b924753j.

[37] Y. Zheng, W. Shi, J. Kong, D. Huang, H.E. Katz, J. Yu, A.D. Taylor, A Cytop Insulating Tunneling Layer for Efficient Perovskite Solar Cells, Small Methods. 1 (2017) 1700244. https://doi.org/10.1002/smtd.201700244.

[38] E.H. Williams, J.A. Schreifels, M. V. Rao, A. V. Davydov, V.P. Oleshko, N.J. Lin, K.L. Steffens, S. Krylyuk, K.A. Bertness, A.K. Manocchi, Y. Koshka, Selective streptavidin bioconjugation on silicon and silicon carbide nanowires for biosensor applications, J. Mater. Res. 28 (2013) 68–77. https://doi.org/10.1557/jmr.2012.283.

[39] Y. Hanada, K. Sugioka, K. Midorikawa, UV waveguides light fabricated in fluoropolymer CYTOP by femtosecond laser direct writing, Opt. Express. 18 (2010) 446. https://doi.org/10.1364/oe.18.000446.

[40] T. Yamada, K. Fukuhara, K. Matsuoka, H. Minemawari, J. Tsutsumi, N. Fukuda, K.

Aoshima, S. Arai, Y. Makita, H. Kubo, T. Enomoto, T. Togashi, M. Kurihara, T. Hasegawa, Nanoparticle chemisorption printing technique for conductive silver patterning with submicron resolution, Nat. Commun. 7 (2016) 1–9. https://doi.org/10.1038/ncomms11402.

[41] R.G. Acres, A. V. Ellis, J. Alvino, C.E. Lenahan, D.A. Khodakov, G.F. Metha, G.G. Andersson, Molecular structure of 3-aminopropyltriethoxysilane layers formed on silanol-terminated silicon surfaces, J. Phys. Chem. C. 116 (2012) 6289–6297. https://doi.org/10.1021/jp212056s.

[42] Y. Don Park, J.A. Lim, H.S. Lee, K. Cho, Interface engineering in organic transistors, Mater. Today. 10 (2007) 46–54. https://doi.org/10.1016/S1369-7021(07)70019-6.

[43] I. Buchwalow, V. Samoilova, W. Boecker, M. Tiemann, Non-specific binding of antibodies in immunohistochemistry: Fallacies and facts, Sci. Rep. 1 (2011). https://doi.org/10.1038/srep00028.

[44] A. Goyon, M. Excoffier, M.C. Janin-Bussat, B. Bobaly, S. Fekete, D. Guillarme, A. Beck, Determination of isoelectric points and relative charge variants of 23 therapeutic monoclonal antibodies, J. Chromatogr. B Anal. Technol. Biomed. Life Sci. (2017). https://doi.org/10.1016/j.jchromb.2017.09.033.

[45] S. BOGOCH, E.S. BOGOCH, Malignin, Anti-Malignin Antibody and Scantag, in: 1983: pp. 337–352. https://doi.org/10.1016/b978-0-08-029815-3.50081-7.

[46] U. Sankilampi, P.O. Honkanen, A. Bloigu, E. Herva, M. Leinonen, Antibody response to pneumococcal capsular polysaccharide vaccine in the elderly, J. Infect. Dis. 173 (1996) 387–393. https://doi.org/10.1093/infdis/173.2.387.

Appendix A. Supporting Information

Organic-based Field Effect Transistors for Protein Detection fabricated by Inkjet-Printing

*Carme Martínez-Domingo, Silvia Conti, Alfredo de la Escosura-Muñiz, Lluís Terés, Arben Merkoçi and Eloi Ramon **

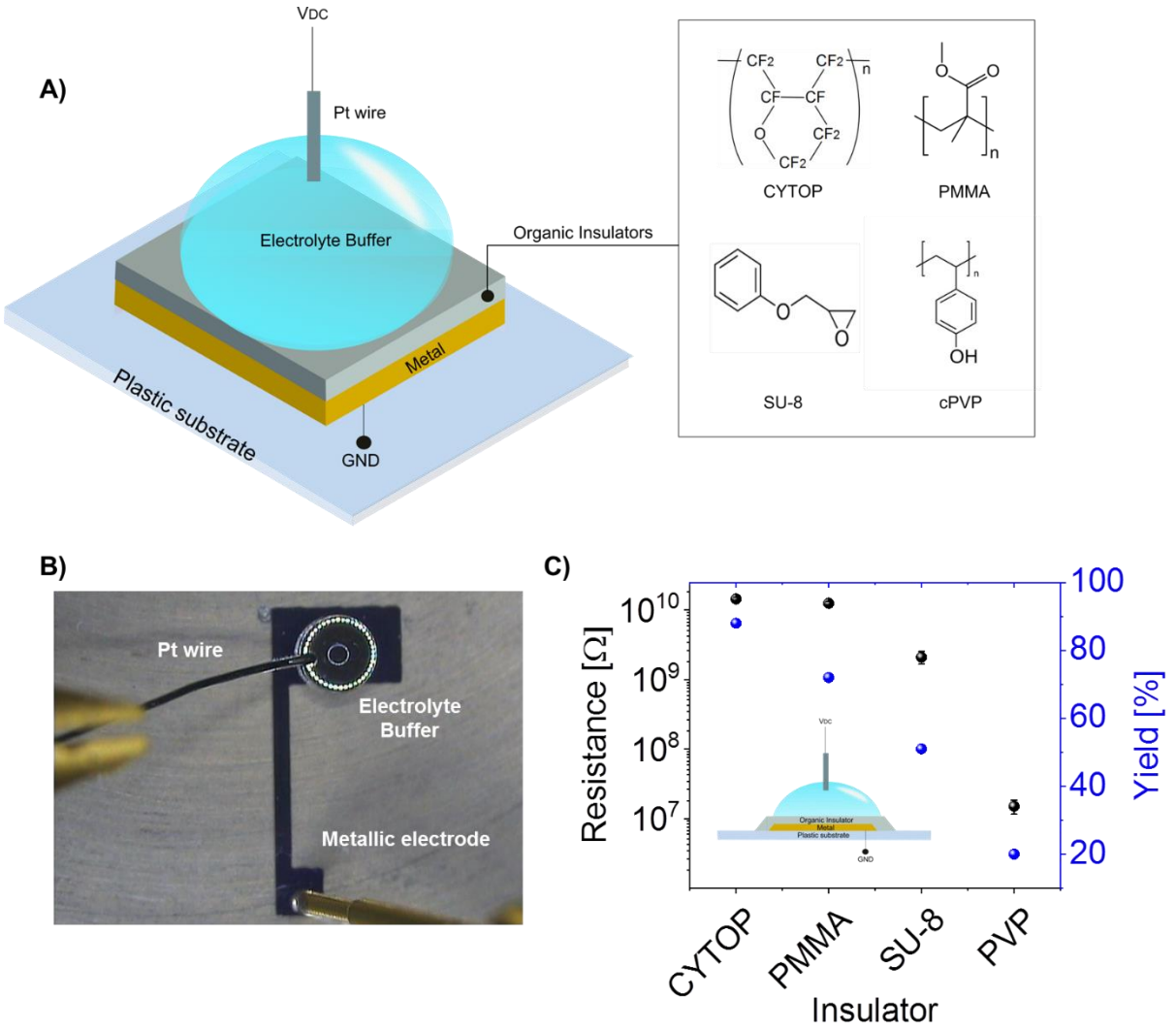

Figure S1. A) Scheme of the MIE structure and molecular structures of the organic insulator used. B) Optical image of the MIE electrical characterization and C) Resistance and device yield for each dielectric studied.

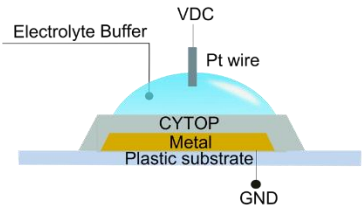

	pH	Electrolyte Buffer	Buffer concentration [mM]
A1	7	PBS	10
A2	5	MES	100
A3	5	MES	50
A4	5	MES	10

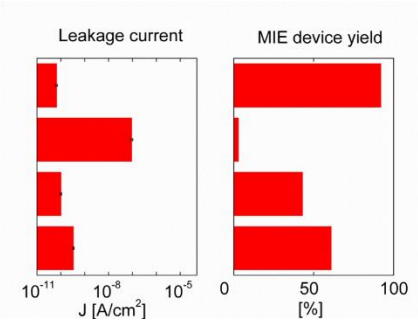

Figure S 2. Scheme of MIE structure using Cytop as an insulator. The table shows the electrolyte buffer and its concentrations. Leakage current and MIE device yield is shown for each buffer used.

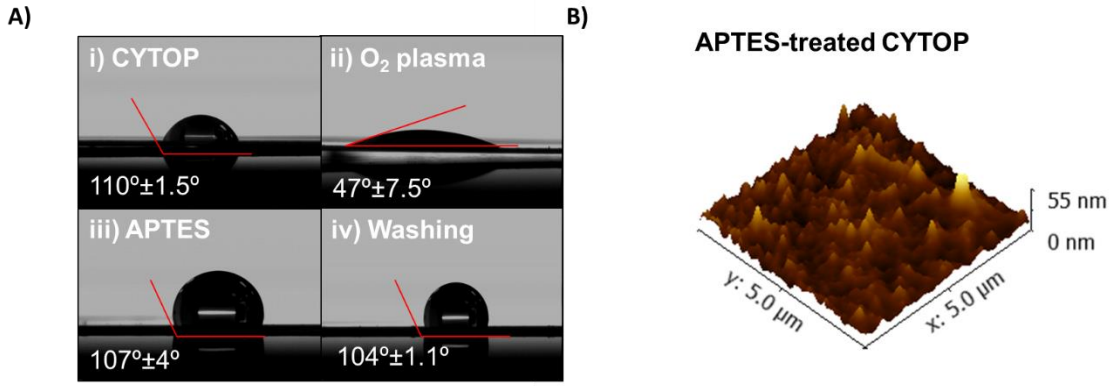

Figure S 3. A) Contact angle measurement for i) Cytop, ii) oxygen treated Cytop, iii) oxygen and APTES-treated Cytop and iv) oxygen and APTES-treated Cytop after washing, B) 3D topographic AFM image for APTES-treated Cytop.

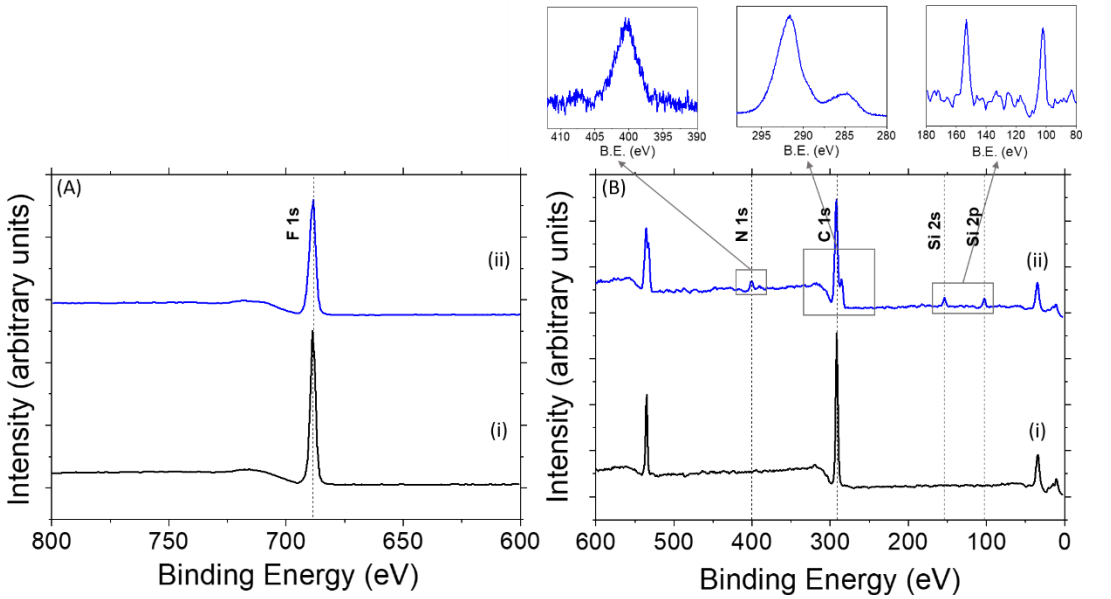

Figure S 4. XPS spectra of CYTOP surface: (i) before and (ii) after APTES functionalization: F 1s (A), N 1s (B), C 1s (B), Si 2s (B), and Si 2p (B). The insets show high-resolution XPS N 1s (left side), C 1s (central), and Si 2s Si 2p (right side) spectra from APTES functionalized CYTOP surface.

Electrical characterization of the BioFET under immobilization protocol

As underlined in the introduction, the decrease/increase in the current is due to the presence of positively/negatively charged molecules that change the surface potential. αHIgG (Isoelectric Point (pI) 6.6-8.5) [1] is negatively charged at the pH of the working buffer (pH 9), so an increase in the current is expected for an increase of the antibody concentration. Human IgG (HIgG) antigen was finally evaluated as a model protein to be detected by the immunosensing system as it is shown in Figure S5.

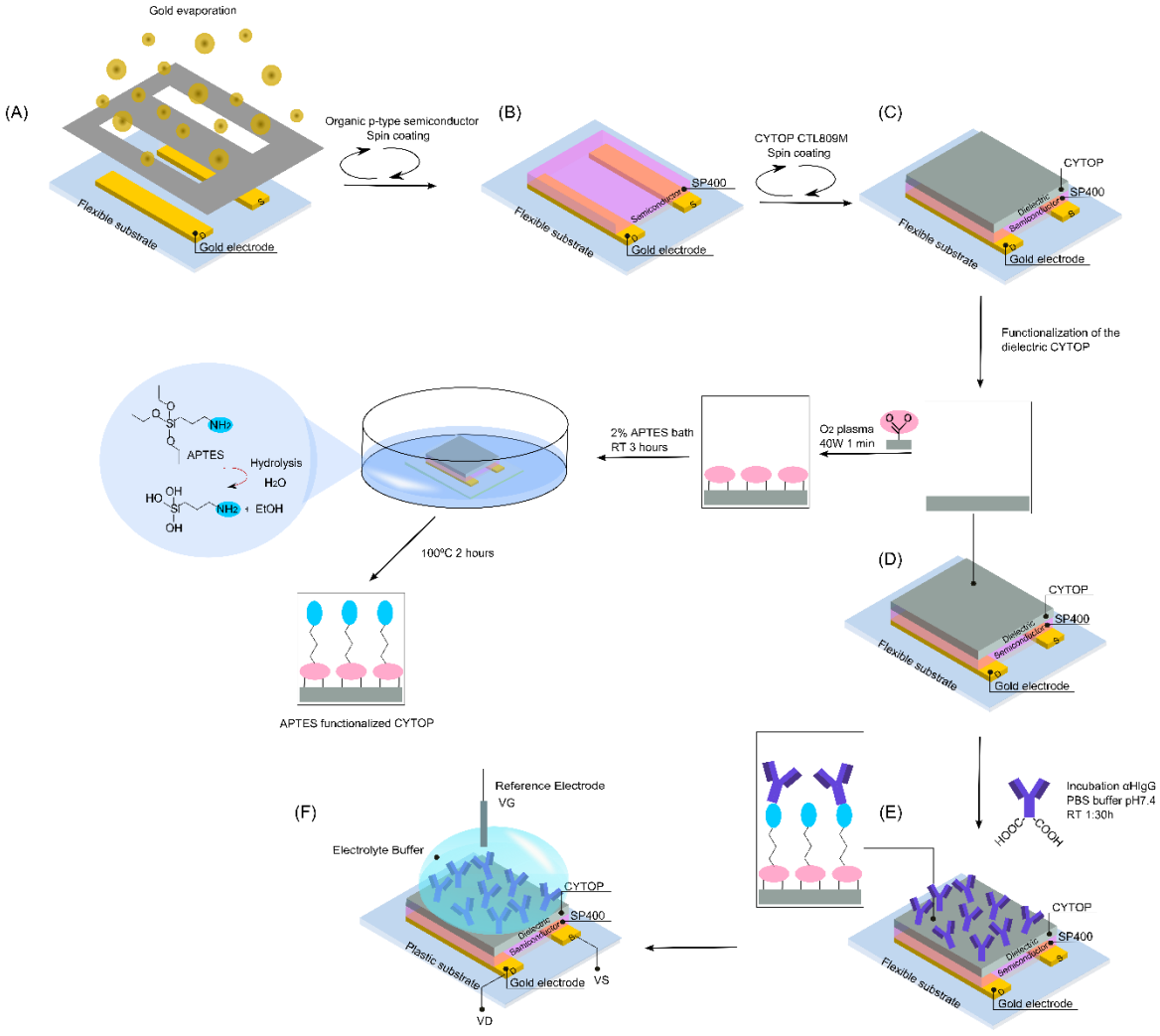

Figure S5. Schematic of the stepwise fabrication and functionalization of the BioFET. A) evaporation of the gold electrodes onto the flexible substrate, B) the OSC is spin-coated onto the electrodes and C) the dielectric Cytop was spin-coated onto the OSC. D) functionalization of the Cytop through oxygen plasma and APTES treatment, E) Incubation of αHIgG and F) electrical characterization of the devices containing the antibodies.

The immunocomplex formation was monitored through drain current measurements. αHIgG antibody concentration was fixed at 400 μg mL^{-1} and non-specific absorptions were avoided by the blocking of the BioFET surface with casein before the incubation of the antigen (see the *experimental section*). **Figure S6.A** shows the schematics of the immunosensing system. Blank assays were performed in the absence of antigen (in PBS solution) while control assays correspond to those performed with an unspecific protein (goat IgG (GIgG)). The percentage change of drain current was evaluated from the transfer curves at the maximum V_{DS} as $\Delta I/I(\%)=[(I_{antibody}-I_0)I_0^{-1}]\cdot 100$ being $I_{antibody}$ and I_0 the drain current with and without the presence of target. Analysis of the results indicates that the current increases when the antibody αHIgG is attached onto the amine-functionalized Cytop film, as expected. It is possible to presume that the negative charges of the αHIgG attract the holes to the transistor channel region increasing the overall current. Moreover, Figure S6.B shows that an increase of 102% in the drain current was observed in the presence of the antigen HIgG due to the immunocomplex formation. A slight increase in the current was recorded for both the blank and the control assays, demonstrating the specificity of the immunosensing system.

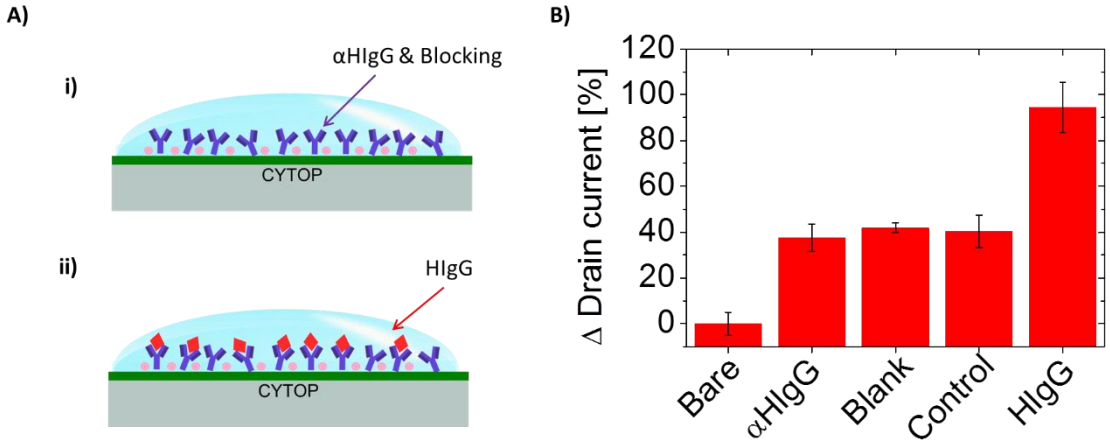

Figure S6. A) Schematic of the stepwise functionalization of the BioFET for: i) immobilization of antibodies αHIgG and the casein as the blocking agent to prevent non-specific absorption; and, ii) immunoreaction with HIgG specific antigen. B) Change of the I_{DS} of the BioFETs for bare BioFET and the BioFET modified with antibody, before and after the immunoreaction with HIgG, as well as for the blank and control assays.

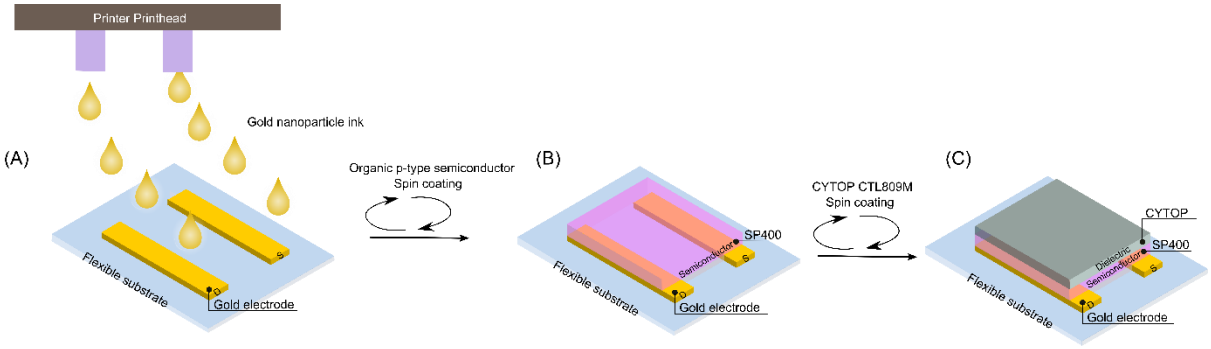

Figure S7. Schematic of the inkjet-printed BioFET fabrication. A) the gold electrodes were patterned by inkjet printing technique using gold nanoparticle ink, B) the OSC is spin-coated onto the electrodes and C) the dielectric Cytop was spin-coated onto the OSC.

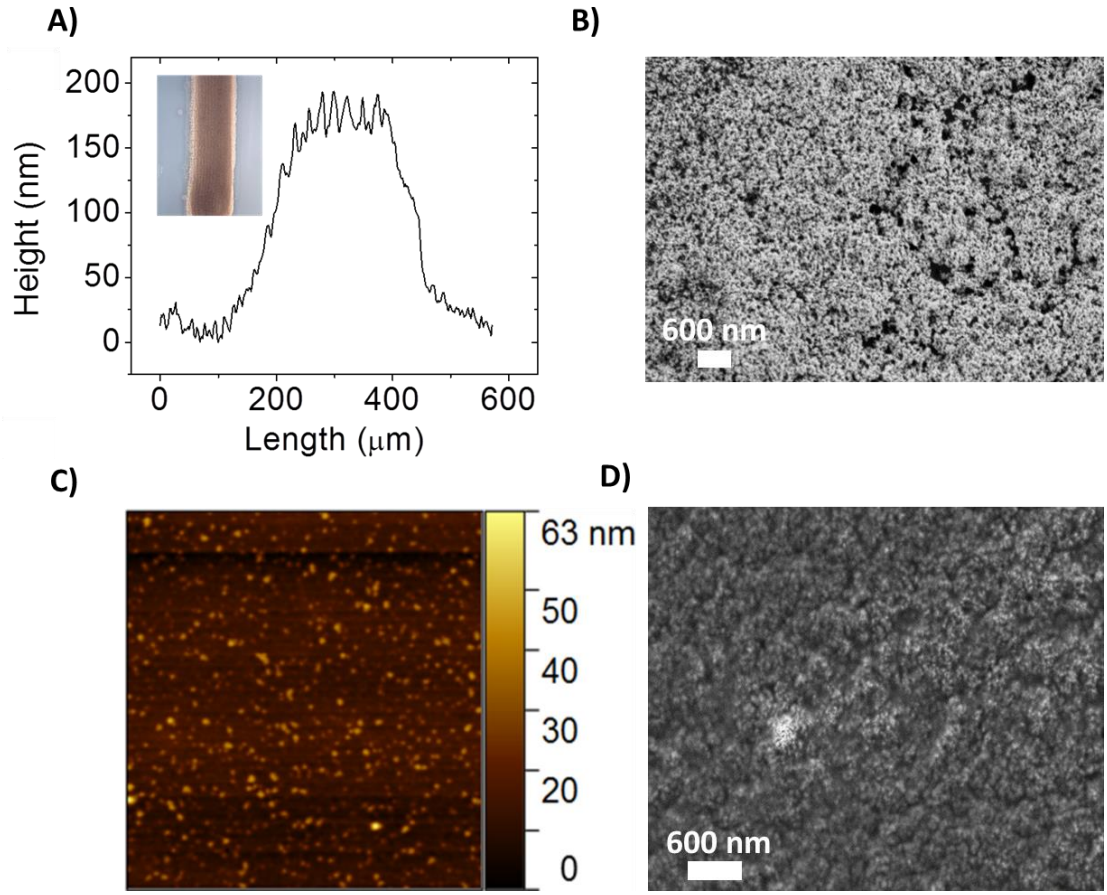

Figure S8. A) Profile measurement of a gold inkjet-printed electrode. Inset: Optical image of the inkjet-printed drain electrode. B) SEM image of a gold inkjet-printed electrode. C) AFM image of the inkjet-printed OSC. D) SEM image of the-inkjet printed OSC.

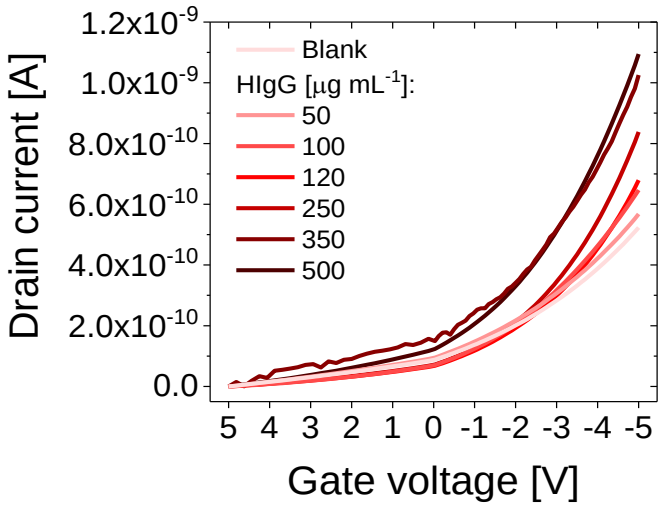

Figure S9. Current-voltage characteristics of the top-gate BioFET without HIgG, referred as blank, and in solutions with increasing HIgG concentrations, ranging from 50 µg mL^{-1} to 500 µg mL^{-1}. The applied drain-source voltage, V_{DS}, is -5V.

TABLES.

Table S1. Cytop profile thickness, surface roughness, leakage current, capacitance and device yield for MIE structure for spin-coating speeds of 500, 1000, 1500 and 2000 rpm.

Spin-coating Speed	**Profile Thickness [µm]**	**RMS roughness [nm]**	**Leakage current at 20V [pA]**	**Capacitance at 1Hz [F/cm^2]**	**Yield [%]**
500 rpm	2.0-3.5	0.38-0.52	12	$25 \cdot 10^{-9}$	83
1000 rpm	0.8-0,9	0.35	32	$2 \cdot 10^{-6}$	88
1500 rpm	0.7-0.8	0.39	310	$2.25 \cdot 10^{-3}$	58
2500 rpm	0.40-0.45	0.45	2300	-	20

Table S2. Electrical parameters of top-gate BioFETs without surface functionalization fabricated with conventional techniques. All the electrical characteristics were measured under a 10 μL PBS droplet placed over the Cytop

Vth [V]	**μ [cm^2/V·s]**	**I_{ON}/I_{OFF}**	**|Ig| [A]**	**Hysteresis [V]**
-1.8±0.33	$(0.78\pm1.6)\cdot10^{-3}$	$(8\pm2)\cdot10^{2}$	$(-40\pm7)\cdot10^{-12}$	$(-15\pm0.2)\cdot10^{-3}$

Table S3. Electrical parameters of top-gate inkjet-printed BioFETs without surface functionalization. All the electrical characteristics were measured under a 10 μL PBS droplet placed over the Cytop

Vth [V]	**μ [cm^2/V·s]**	**I_{ON}/I_{OFF}**	**|Ig| [A]**	**Hysteresis [V]**
-0.5±0.1	$(0.9\pm0.05)\cdot10^{-5}$	69±18	$(-9.6\pm0.1)\cdot10^{-12}$	(-0.87±0.12)

Table S4. Comparative table of the related top-gated BioFET sensors based on hydrophobic polymers as gate dielectrics and based on inorganic gate dielectrics.

Reference	Analyte/ LOD	Ionic strengh	Substrate	Fabrication technique	Gate dielectric layer	Transistor architecture
Our work	HIgG/ 5.71 µg mL^{-1}	10 mM PBS	PEN	Inkjet-printing and spin coating	Hydrophobic: Cytop	Top-gate
A [2]	BSA/ 1.21 µM	DI water	Silicon	Conventional	Hydrophobic: Cytop	Top-gate
B [3]	Glial fibrillary acidic protein (GFAP)/ 20 pM	50 mM PBS	Silicon	Conventional	Hydrophobic: Cytop	Top-gate
C [4]	Streptavidin/ 10 nM	10 mM PBS	Silicon	Conventional	Hydrophobic: Phospholipid	Top-gate
D [5]	BSA/ 33 µg mL^{-1}	10 mM PBS	Silicon	Conventional	Hydrophobic: Cytop	Top-gate
E [6]	BSA/ K_A= $1.1*10^{-7}$ M^{-1}	10 mM ABS	Silicon	Conventional	Hydrophobic: Perfluor-1,3-dimethylcyclohexan (PFDMCH)	Top-gate
F [7]	IgG/ 10 fM	-	Silicon	Conventional	Inorganic: SiO_2	Bottom gate
G [8]	IgG/ 4 nM	D-PBS	PEN	Conventional	Inorganic: AlO_x +SAM	Extended and bottom gate

Relevant biosensors based on field-effect transistors are summed up in Table S4. Different architectures have been explored such as top-gate, bottom-gate, and extended-gate. Each architecture implies and, at the same time, constraints the materials and fabrication technique that can be used, since the morphology of the different layers affects the device performance. From the data, it is possible to notice that silicon wafer is the most commonly used substrate. Thanks to its capability to handle high-temperature processes, this choice favors the use of conventional techniques needed for the deposition of highly ordered organic materials, which are not so trivial to obtain with solution approaches.[8] In Table S4, the main aspect to be compared is the transducer: top-gate architectures use hydrophobic gate dielectric layers, whereas inorganic semiconductors and metals are employed in bottom and extended gate architectures, respectively. Although immunodetection is proven for every hydrophobic layer reported in these works, there are some differences in the insulator functionalizations and the

sensing mechanisms. A common problem for all the devices is the difficulty in obtaining an efficient graft of the hydrophilic bio-recognition elements to the highly hydrophobic dielectric layers. Several methods have been proposed for the functionalization. From ref. B to ref. E (Table S4), the antibody linkage is achieved via thermal deposition, plasma enhanced chemical vapour deposition (PE-CVD), and physical vapour deposition (PVD). In ref. F (Table S4) and ref. G the formation of the bio-receptor layer is performed directly onto an inorganic semiconductor such as silicon nanowires (SiNWs) or an Au gate electrode. In the former, organic solvents and EDC/NHS chemistry is used to attach the biomolecules, while in the latter, SAM molecules are employed. The direct transfer of these functionalization protocols to OSCs can be detrimental for the semiconductor performance.[9] The introduction of hydrophobic dielectrics to protect them is, thus, necessary. It is worth noticing that the majority of the reported functionalization procedures has been done in vapour phase to assure less impact to the transistor but increasing the fabrication complexity. In counterpart, our BioFET is aimed to cope with simpler solution based functionalization protocols as organic solvents and oxygen plasma. Besides these points, the main difference between our device and the other works is that, in our case, the bio-recognition event is detected by a perturbation of the coupling between the gate and the OSC due to a variation of the field-effect at the gate.

While screen printing remains the most important and commonly used technique for the fabrication of biosensors based on electrodes, more recently inkjet-printing has also been proposed for device fabrication. Typically, biosensors are electrochemical devices based on three-electrode systems.[10] More sophisticated electronic approaches are still underrepresented in literature. Elegant and interesting outcomes have been proposed to palliate and overcome the current limitations of conventional and bulky techniques for diagnosis and analytical applications using screen printed three-electrode devices. Their

simplicity and robustness in terms of fabrication have propelled them in front of other biosensors. Currently the research appears unbalanced between these two printing techniques. From a technological evaluation, inkjet printing presents higher resolution of the printing layers up to the nanoscale range and, it can be potentially employed for the fabrication of biosensors based on semiconductor devices such as diodes and transistors. This manuscript should be intended as a contribution to the field of biosensors based on electronic devices fabricated using inkjet printing. As it can be noticed in Table S4, there is a lack of printed electronic devices. Moreover, an interesting outcome of this work is the development of a reliable transducer based on inkjet printed organic materials, which adds interesting functionalities to the organic electronics field. It is worth mentioning that the developed device can host label-free biomolecules, in contrast to what commonly occurs in three-electrode approaches. Another interesting aspect of this device is that the BioFET is an intrinsic amplifier of the signal. Finally, as an inherent feature of any electrochemical sensor, the BioFET device can also be miniaturized and it is compatible with portable electrical readout equipment. From a practical point of view, the BioFET accomplishes the requirements of the current technology used for the fabrication of organic electronic components, already present in the technological market, and it can be easily adapted to the emergent low-cost technology demand.

Supporting Information Refences:

[1] A. Goyon, M. Excoffier, M.C. Janin-Bussat, B. Bobaly, S. Fekete, D. Guillarme, A. Beck, Determination of isoelectric points and relative charge variants of 23 therapeutic monoclonal antibodies, J. Chromatogr. B Anal. Technol. Biomed. Life Sci. (2017). https://doi.org/10.1016/j.jchromb.2017.09.033.

[2] J. Choi, H.G. Jeon, O.E. Kwon, I. Bae, J. Cho, Y. Kim, B. Park, Improved output characteristics of organic thin film transistors by using an insulator/protein overlayer and their applications, J. Mater. Chem. C. 3 (2015) 2603–2613. https://doi.org/10.1039/c4tc02823f.

[3] W. Huang, K. Besar, R. LeCover, P. Dulloor, J. Sinha, J.F. Martínez Hardigree, C. Pick, J. Swavola, A.D. Everett, J. Frechette, M. Bevan, H.E. Katz, Label-free brain injury biomarker detection based on highly sensitive large area organic thin film transistor with hybrid coupling layer, Chem. Sci. 5 (2014) 416–426. https://doi.org/10.1039/C3SC52638K.

[4] M. Magliulo, A. Mallardi, M.Y. Mulla, S. Cotrone, B.R. Pistillo, P. Favia, I. Vikholm-Lundin, G. Palazzo, L. Torsi, Electrolyte-gated organic field-effect transistor sensors based on supported biotinylated phospholipid bilayer, Adv. Mater. 25 (2013) 2090–2094. https://doi.org/10.1002/adma.201203587.

[5] H.U. Khan, J. Jang, J.-J. Kim, W. Knoll, Effect of passivation on the sensitivity and stability of pentacene transistor sensors in aqueous media, Biosens. Bioelectron. 26 (2011) 4217–4221. https://doi.org/10.1016/j.bios.2011.03.031.

[6] H.U. Khan, J. Jang, J.-J. Kim, W. Knoll, In Situ Antibody Detection and Charge Discrimination Using Aqueous Stable Pentacene Transistor Biosensors, J. Am. Chem. Soc. 133 (2011) 2170–2176. https://doi.org/10.1021/ja107088m.

[7] X. Gong, R. Zhao, X. Yu, High sensitive detections of Norovirus DNA and IgG by using multi-SiNW-FET biosensors, 2015 Transducers - 2015 18th Int. Conf. Solid-State Sensors, Actuators Microsystems, TRANSDUCERS 2015. (2015) 1537–1540. https://doi.org/10.1109/TRANSDUCERS.2015.7181230.

[8] T. Minamiki, T. Minami, R. Kurita, O. Niwa, S.I. Wakida, K. Fukuda, D. Kumaki, S. Tokito, A label-free immunosensor for IgG based on an extended-gate type organic field effect transistor, Materials (Basel). 6 (2014) 6843–6852. https://doi.org/10.3390/ma7096843.

[9] R. Porrazzo, S. Bellani, A. Luzio, C. Bertarelli, G. Lanzani, M. Caironi, M.R. Antognazza, Field-effect and capacitive properties of water-gated transistors based on polythiophene derivatives, APL Mater. 3 (2015). https://doi.org/10.1063/1.4900888.

[10] V. Perumal, U. Hashim, Advances in biosensors: Principle, architecture and applications, J. Appl. Biomed. 12 (2014) 1–15. https://doi.org/10.1016/j.jab.2013.02.001.